Quantal Transmitter Release at Somatic Motor-Nerve Terminals: Stochastic Analysis of the Subunit Hypothesis

M. R. Bennett,* L. Farnell,‡ and W. G. Gibson‡
*The Neurobiology Laboratory, Department of Physiology, and ‡The School of Mathematics and Statistics, University of Sydney, New South Wales, 2006, Australia

ABSTRACT Here we analyze the problem of determining whether experimentally measured spontaneous miniature end-plate currents (MEPCs) indicate that quanta are composed of subunits. The properties of MEPCs at end plates with or without secondary clefts at the neuromuscular junction are investigated, using both stochastic and deterministic models of the action of a quantum of transmitter. It is shown that as the amount of transmitter in a quantum is increased above about 4000 acetylcholine (ACh) molecules there is a linear increase in the size of the MEPC. It is possible to then use amplitude-frequency histograms of such MEPCs to detect a subunit structure, as there is little potentiation effect above 4000 ACh molecules. Autocorrelation and power spectral analyses of such histograms establish that their subunit structure can be detected if the coefficient of variation of the subunit size is less than about 0.12 or, if electrical noise is added, about 0.1. Positive gradients relate the rise time and half-decay times of MEPCs to their amplitude, even in the absence of potentiating effects; these gradients are shallower at motor nerve terminals that possess secondary clefts. The effect of asynchronous release of subunits is also investigated. The criteria determined by this analysis for identifying a subunit composition in the quantum are applied to an amplitude-frequency histogram of MEPCs recorded from a small group of active zones at a visualized amphibian motor-nerve terminal. This did not provide evidence for a subunit structure.

INTRODUCTION

The concept of spontaneous miniature end-plate currents (MEPCs) or the quantum of transmitter release comprising subunits arose from a consideration of the amplitude-frequency histograms of MEPCs observed during development, which often show peaks that on closer inspection appear to occur at regular intervals (Bennett and Pettigrew, 1975; Kriebel and Gross, 1974). Such subunit peaks were subsequently observed in adult mammalian and amphibian end plates by Kriebel and his colleagues (Kriebel et al., 1982; Carlson and Kriebel, 1985; Vautrin and Kriebel, 1991) but not by others (Bevan, 1976; Magleby and Miller, 1981). Magleby and Miller produced evidence that these subunit peaks might be a statistical artefact, but this was challenged by Vautrin (1986), who used both autocorrelation and spectral density analysis of the amplitude-frequency histograms to show that the peaks were unlikely to be statistical artefacts. A point of difficulty that is frequently raised with respect to the interpretation of these peaks as being due to subunits that comprise the quantum is that the variance of the individual peaks does not seem to increase much, if at all, as the number of subunits increases (Katz, 1977; Bevan, 1976). Another possible difficulty with this interpretation of the peaks is that if release of subunits occurs from the same site on the nerve terminal then it might be expected that considerable potentiation of the effects of one subunit due to the preceding subunit will occur, so that peaks should be spread out at increasing intervals in the histograms and with an increasing variance, because of this potentiation effect (Girod et al., 1993).

A different approach to the question of whether quanta are composed of subunits relates to the small proportion of MEPCs that possess rise times that are very long compared with that of the normal MEPC and which may even show inflections on their rising phases. The different shapes of MEPCs can easily be accommodated within the subunit hypothesis as being due to different patterns of asynchronous release, as has been argued quantitatively for the MEPCs at the electroplaque (Girod et al., 1993) and for synaptic currents at hippocampal synapses (Vautrin et al., 1993). The present work examines the conditions under which the time course and amplitude of the normal fast MEPC may reveal subunits, using a stochastic model of the interaction of the transmitter with the postsynaptic receptors developed by Bartol et al. (1991) and a deterministic model due to Wathey et al. (1979).

METHOD

Two methods have been used to calculate the currents resulting from transmitter release. The first, following the work of Wathey et al. (1979), is a deterministic one in which the differential equations governing diffusion and the kinetics of interaction between ACh and receptors and enzyme are solved for a particular geometry. The second, following the work of Bartol et al. (1991), is a Monte Carlo simulation in which the motions of individual molecules of ACh are followed as they diffuse in the synaptic cleft and bind to receptors or enzymes. The relative merits of the two methods have been discussed by Bartol et al. (1991): the differential equation approach is pref-

Received for publication 24 May 1995 and in final form 23 October 1995.
Address reprint requests to Professor Max Bennett, Neurobiology Laboratory, F13, University of Sydney, New South Wales 2006, Australia. Tel.: 61-2-351-3034; Fax: 61-2-351-4740; E-mail: maxb@physiol.su.oz.au.

0006-3495/96/02/654/00 $2.00

erable if the geometry is simple and one requires only average values; the Monte Carlo method is more easily adapted to complicated geometries, and since it models the stochastic situation it gives the magnitude of the fluctuations that could be expected in an experimental situation. In this paper, both the deterministic and Monte Carlo methods have been used in the case of the flat end plate, but only the Monte Carlo method has been used for the more complicated geometry of the end plate with secondary clefts, because it is more readily adapted to such cases.

Geometry of the synaptic cleft

The motor-nerve terminal in some species possesses only primary clefts, for example, slow fibers in lizards, snakes, and amphibia (Heuser and Reese, 1977) and the terminals on electroplaques of fish (Garcia-Segura et al., 1986). Indeed, the autonomic motor-nerve terminals on smooth and cardiac muscles are also bereft of secondary clefts (Bennett, 1972). Such terminals are represented as flat plates, either circular or square, tiled with receptors as shown in Fig. 1 *A*.

The motor-nerve terminal in other species consists of a large number of boutons or varicosities, about one to several microns in diameter, which in the case of those on twitch fibers possess both primary and secondary clefts. This is the case for both lizards (Land et al., 1980; Walrond and Reese, 1985) and snakes (Hartzell et al., 1975), with an active zone clearly delineated on the prejunctional membrane opposite the secondary cleft. This is in contrast to the motor-nerve

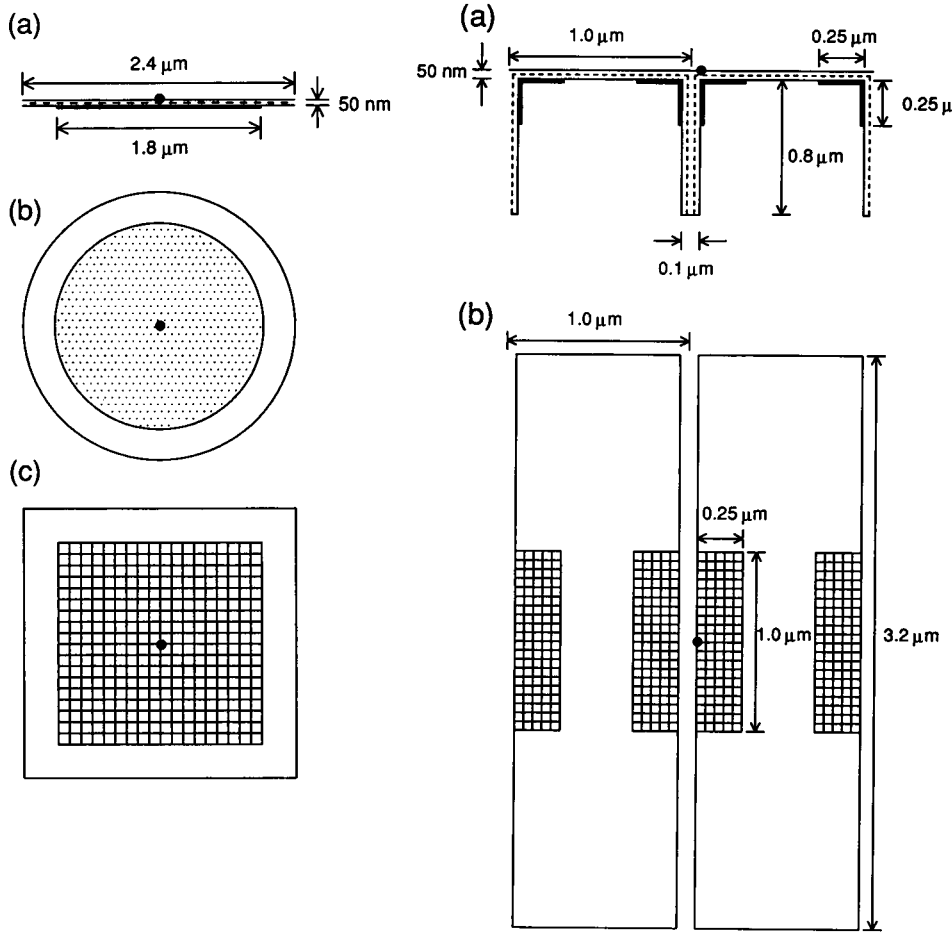

FIGURE 1 Geometry of the neuromuscular junctions analyzed in the present work. (*A*) Junction at the active zone without secondary clefts. (*a*) Cross section through the center of the receptor patch. (*b*) Plan view of the circular case, as used in the deterministic method. (*c*) Plan view of the square case, as used in the Monte Carlo method. The junction is modeled as two parallel plates 50 nm apart and of extension 2.4 μm. The receptor patch is shown as a bold line in *a*, as a dotted area in *b*, and as a hatched area in *c*, each being of extension 1.8 μm; the receptor patch in *c* is tiled at a density of 8200 tiles/μm^2, with each tile containing one receptor molecule. Acetylcholinesterase is located in a sheet of the same area as the junction, placed midway between the presynaptic and postsynaptic membranes and indicated by a broken line in *a*. Transmitter is released from above the center of the receptor patch (●). (*B*) Junction at the active zone with secondary clefts. (*a*) Cross section through the center of the receptor patch. (*b*) Plan view. The primary cleft is of width 50 nm, and the secondary clefts are of width 0.1 μm. The receptors are in rectangular patches 0.25 μm by 1.0 μm placed both in the primary cleft as indicated by the hatched areas in *b* and down the sides of the secondary clefts as indicated by bold lines in *a*. The patches are tiled at a density of 8200 tiles/μm^2, and each tile contains one receptor molecule. Acetylcholinesterase is located in sheets placed midway between presynaptic and postsynaptic membranes in the primary cleft and between the postsynaptic membrane and the central line in the secondary clefts, as indicated by the broken lines in *a*; their longitudinal extension is that of the receptor patch, namely 1.0 μm. Transmitter is released from above the center of a receptor patch and at the edge of a secondary cleft (●).

terminals on the twitch fibers of amphibia and mammals, which have branches that do not possess varicosities and are approximately of uniform diameter; active zones occur every 1 μm or less along the length of the branches, opposite both primary and secondary clefts (Heuser and Reese, 1977). At all these junctions acetylcholine receptors (AChRs) are found on the lips of the secondary clefts as well as in the depth of these clefts; this situation is illustrated in Fig. 1 *B*.

Interaction kinetics

The kinetics of ACh interaction with the receptors is governed by

$$2A + R \underset{k_{-1}}{\overset{2k_1}{\rightleftarrows}} A + AR \underset{2k_{-2}}{\overset{k_2}{\rightleftarrows}} A_2R' \underset{\alpha}{\overset{\beta}{\rightleftarrows}} A_2R^*, \quad (1)$$

where A is an ACh molecule, R is a receptor molecule, AR is the singly liganded channel, A_2R' is the doubly liganded channel in the closed conformation, and A_2R^* is the doubly liganded channel in the open conformation. In practice (cf. Bartol et al., 1991) Eq. 1 can be simplified to

$$2A + R \underset{k_{-1}}{\overset{2k_1}{\rightleftarrows}} A + AR \underset{2k_{\text{eff}}}{\overset{k_2}{\rightleftarrows}} A_2R, \quad (2)$$

where $k_{\text{eff}} = \alpha/(\alpha + \beta)k_{-2}$ and the number of open channels is found by multiplying the number of doubly liganded channels (A_2R) by $\beta/(\alpha + \beta)$. Note that A_2R signifies all doubly liganded channels; that is, it includes the closed channel A_2R' and the open channel A_2R^*. The interaction of ACh with esterase is governed by

$$A + E \overset{k_3}{\rightarrow} AE \overset{k_4}{\rightarrow} E + Q, \quad (3)$$

where E denotes the enzyme and Q the final products of hydrolysis.

If we ignore spatial effects, then Eqs. 2 and 3 lead to the following kinetic equations for the concentrations of the various molecules:

$$\frac{d[AR]}{dt} = 2k_1[A][R] - k_{-1}[AR] + 2k_{\text{eff}}[A_2R] - k_2[A][AR] \quad (4)$$

$$\frac{d[A_2R]}{dt} = k_2[A][AR] - 2k_{\text{eff}}[A_2R] \quad (5)$$

$$\frac{d[AE]}{dt} = k_3[A][E] - k_4[AE] \quad (6)$$

$$\frac{d[Q]}{dt} = k_4[AE] \quad (7)$$

where

$$[A] = [A]_0 - [AR] - 2[A_2R] - [AE] - [Q] \quad (8)$$

$$[R] = [R]_0 - [AR] - [A_2R] \quad (9)$$

$$[E] = [E]_0 - [AE], \quad (10)$$

and $[X]_0$ denotes the initial concentration of substance X.

Deterministic method

The concentration of ACh is a function of spatial position and time, $[A] = [A](r, x, z, t)$, and one starts by writing

$$\frac{\partial[A]}{\partial t} = \frac{\partial[A]}{\partial t}\bigg|_{\text{diffusion}} + \frac{\partial[A]}{\partial t}\bigg|_{\text{kinetics}}. \quad (11)$$

The diffusion term is the solution of

$$\frac{\partial[A]}{\partial t}\bigg|_{\text{diffusion}} = D\nabla^2[A], \quad (12)$$

where D is the diffusion coefficient and ∇^2 is the Laplacian operator. In practice we only apply this method to the case of radially symmetric diffusion over a disc (Fig. 1 *Ab*), so Eq. 4 reduces to the one-dimensional form

$$\frac{\partial[A]}{\partial t}\bigg|_{\text{diffusion}} = D\left(\frac{\partial^2[A]}{\partial r^2} + \frac{1}{r}\frac{\partial[A]}{\partial r}\right), \quad (13)$$

where r is the radial distance. The kinetics term is, from Eq. 8,

$$\frac{\partial[A]}{\partial t}\bigg|_{\text{kinetics}} = -\frac{\partial[AR]}{\partial t} - 2\frac{\partial[A_2R]}{\partial t} - \frac{\partial[AE]}{\partial t} - \frac{\partial[Q]}{\partial t}, \quad (14)$$

where the partial derivatives on the right-hand side are given by Eqs. 4 to 7, with d/dt replaced by $\partial/\partial t$ in each case. The ACh concentration [A], as a function of position and time, is now found by (numerically) solving the above set of coupled differential equations under appropriate initial conditions and boundary conditions.

Monte Carlo method

The Monte Carlo method involves following the motion of each molecule as it executes a random walk in free space, is reflected from presynaptic and postsynaptic membranes, and binds to or unbinds from receptor molecules. A detailed description and justification of the Monte Carlo method, as applied to the release of ACh in the neuromuscular junction, has been given by Bartol et al. (1991), and the present calculation closely follows their methods. Two geometries are considered, one without secondary clefts (Fig. 1 *A*) and the other with secondary clefts (Fig. 1 *B*). In each case, receptors are found in patches on the postsynaptic membrane, and these patches are subdivided into tiles of appropriate size, each tile containing one receptor. The actual size of the receptor is 10 nm^2, which is much smaller than the tile size. Acetylcholinesterase is located in sheets above the

postsynaptic membrane, as shown by the broken lines in Fig. 1, *Aa* and *Ba*.

Quanta of ACh are released from the presynaptic membrane, either from a point above the center of the receptor patch (marked with a black spot in Fig. 1 *A*) or from a point above the edge of a secondary cleft and midway along a receptor patch (marked with a black spot in Fig. 1 *B*). Each molecule is moved randomly, using a time step of 0.75 μs. The algorithms and formulas used are as described by Bartol et al. (1991).

Parameter values

The parameter values used in the calculations reported here are, unless otherwise stated, the same as those used by Bartol et al. (1991) (see also Land et al., 1980); for convenience, they have been collected in Table 1. On some occasions the kinetic parameters given in Auerbach (1993) have been used, as also summarized in Table 1. When this is the case, it is explicitly stated in the figure legends.

Summation of subunit responses

We can investigate theoretically the variability expected in the total response when a number of subunits of transmitter are released simultaneously. Let N units be released, and suppose that the rth such unit causes a postsynaptic current X_r. Suppose that N is a binomially distributed random variable with parameters n and p, and that the X_r's are independent identically distributed normal random variables, with mean μ and variance σ^2. Suppose further that experimental noise can be represented as an additive normally distributed random variable Z with mean 0 and variance $\tilde{\sigma}^2$. The total response is

$$W = X_1 + X_2 + \cdots + X_N + Z \qquad (15)$$

and it follows from the above assumptions that W has density function

$$fw(w) = \sum_{r=1}^{n} \frac{1}{\sigma_r \sqrt{2\pi}} \exp\left(-\frac{(w - r\mu)^2}{2\sigma_r^2}\right) b(r; n, p) \qquad (16)$$

where $\sigma_r^2 = r\sigma^2 + \tilde{\sigma}^2$ and $b(r; n, p)$ is the binomial probability function.

Recording MEPCs from visualized motor-nerve terminals

Toads (*Bufo marinus*) weighing 24–40 g were housed in tanks fitted with 15% ultraviolet lights (Phillips, Grohux) that were left on for 16 h per day. The temperature of the room was maintained at 25–30°C, and the animals were fed a mixture of mincemeat and brittle three times per week. Animals were anaesthetized with tricaine methanesulfonate (Rural Chemical Industries Australia) and then killed by a cervical fracture. Both iliofibularis muscles together with their nerve supplies were dissected free from surrounding connective tissue and tendinous insertions. They were pinned (in a bath of 3 ml capacity) on Sylgard with the ventral surface up and stretched to approximately 110% of their resting length in the limb. The bath was continuously perfused at room temperature (16 ± 2°C) with a modified Ringer solution of the following composition (mM): Na^+, 117.0; K^+, 3.0; Mg^{2+}, 2.0; Cl^-, 103.1; $H_2PO_4^-$, 0.64; HPO_4^{2-}, 9.7; Ca^{2+}, 0.25–0.4; glucose, 7.8. $[Ca^{2+}]_0$ was changed by altering the amount of $CaCl_2$ dissolved in the Ringer solution supplying the bath. The solution was gassed continuously with 95% O_2 and 5% CO_2, and the pH was maintained between 7.2 and 7.5.

The isolated nerve muscle preparations were first bathed for 30 s in 0.1 μM of the fluorescent dye 3,3-diethyloxardicarbocyanine iodide ($DiOC_2(5)$) as previously described (Bennett et al., 1986) and then thoroughly washed with Ringer solution. End plates were chosen by viewing the fluorescent terminals on a video monitor attached via an

TABLE 1 Values of parameters used in the calculations

Quantity	Symbol	Value (Bartol)	Value (Auerbach)
Diffusion coefficient	D	6.5×10^{-6} cm^2 s^{-1}	
Rate constants for binding to receptors	k_1	2.6×10^7 M^{-1} s^{-1}	5.6×10^7 M^{-1} s^{-1}
	k_2	2.6×10^7 M^{-1} s^{-1}	29.6×10^7 M^{-1} s^{-1}
Rate constants for unbinding from receptors	k_{-1}	4120 s^{-1}	2507 s^{-1}
	k_{-2}	4120 s^{-1}	13655 s^{-1}
Rate constants for conformational change	α	2500 s^{-1}	529 s^{-1}
	β	22500 s^{-1}	30000 s^{-1}
Rate constant for binding to esterase	k_3	5.2×10^7 M^{-1} s^{-1}	
Rate constant for hydrolysis	k_4	3.6×10^3 s^{-1}	
Receptor density		8200 μm^{-2}	
Esterase density		3500 μm^{-2}	

image-intensifier camera (Panasonic National) to an Olympus (BH2) fluorescent microscope. Extracellular recordings were obtained using microelectrodes with a diameter of about 6 μm that were filled with bath solution. These were placed in the loose-patch mode over selected portions of the visualized terminal branches. MEPCs were collected using an IBM-AT microcomputer and P-clamp software (Axon Instruments).

RESULTS

Relation between the temporal characteristics of quantal currents and the amount of ACh in a quantum

Solution of the stochastic or deterministic equations for the diffusion of ACh secreted in a quantum from a single release site on a motor-nerve terminal, and its subsequent reaction with AChR and cholinesterase, allows simulation of both the spatial distribution of receptors with doubly bound acetylcholine molecules (A_2R) that give rise to open channels (A_2R^*) (Fig. 2) and the temporal characteristics of the MEPCs that arise as a consequence of the open channels (Fig. 3). There is a nearly linear relationship between the rise time of the MEPC (taken as 20–80% of the peak value of A_2R^* formation) and the peak size of the MEPC (which is proportional to the peak value of A_2R^*) as the amount of ACh in a quantum increases at active zones without secondary clefts (Fig. 4 *A*). Both methods of calculation (Monte Carlo and deterministic) show that the gradient of this relationship is about 1 μs/80 A_2R^* (Fig. 4 *A*). The linear relationship between the time to peak (taken as the interval between the foot of the MEPC and its peak) and the peak A_2R^* has a gradient of 1 μs/46 A_2R^* (Fig. 4 *B*). There is also an approximately linear relationship between the time for half-decay of the MEPC (that is, the time from the peak A_2R^* formation to the half-decay point of this A_2R^*) and the peak size of the currents as the amount of ACh in a quantum increases above a certain minimum amount (Fig. 4 *C*), whether this is calculated by means of the stochastic or deterministic equations; this gradient is about 1 μs/100 A_2R^*.

The quantitative relationship between the temporal properties of the MEPCs and their peak amplitudes is different for quantal release at active zones with secondary clefts compared to those without. At active zones with secondary clefts the rise time of the MEPC increases along a shallower gradient with an increase in the peak size of the MEPC due to an increase in the amount of ACh in a quantum (Fig. 5 *A*), namely at 1 μs/185 A_2R^*. The gradient for the time to peak of the MEPC versus its peak amplitude is 1 μs/135 A_2R^* (Fig. 5 *B*). There is also a shallower gradient for the relationship between the half-decay time of the MEPC and the peak size of the MEPC of 1 μs/73 A_2R^* (Fig. 5 *C*). It seems then that the distribution of receptors at secondary clefts in an end plate compared with

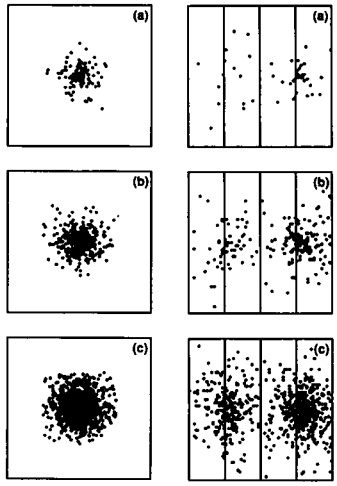

FIGURE 2 A, the spatial spread of A_2R^* over a square of receptors opposite the active zone of a bouton at the time of peak A_2R binding after the release of different amounts of ACh in a quantum. The square shown is 1.8 μm on a side and represents the receptor patch shown in Fig. 1 *Ac*; each A_2R^* molecule is indicated by a filled circle. The number of molecules in a quantum is 2000 (*a*), 4000 (*b*), or 8000 (*c*). (*B*) The spatial spread of A_2R^* over receptors opposite the active zone of an end plate at the time of peak A_2R binding after the release of different amounts of ACh in a quantum. The square shown is 1.0 μm on a side and represents receptor patches shown in the central section of Fig. 1 *B*: it is divided into four rectangles, each of dimension 1.0 μm × 0.25 μm, which represent, from left to right, the lip of a synaptic fold in the primary cleft, the inside face of the fold in the secondary cleft, the opposite face of the fold in the secondary cleft, and the adjacent lip of the fold in the primary cleft. Release of ACh occurs opposite the midpoint of the inside edge of the fourth rectangle. Each A_2R^* molecule is indicated by a filled circle; the number of molecules in a quantum is 2000 (*a*), 4000 (*b*), or 8000 (*c*).

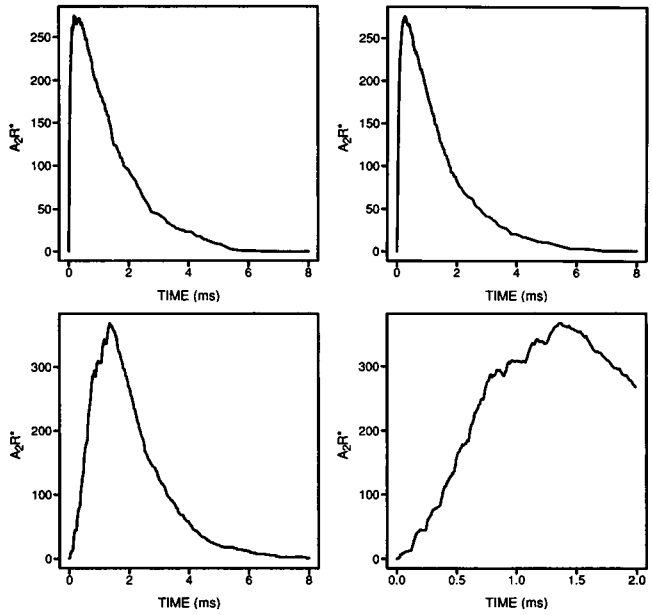

FIGURE 3 The time course of simulated MEPCs at end plates with secondary clefts under three different conditions of temporal release of quantal subunits; the ordinate gives the number of open channels A_2R^*, which is proportional to the current. (*A*) Synchronous release of 5 subunits of ACh, each subunit containing 1000 molecules. (*B*) Release of 5 subunits at 5 μs apart. (*C*) Release of 7 subunits at 120-μs intervals, then 3 at 180-μs intervals. (*D*) As for *C* but on an expanded time scale, showing more clearly the inflections on the rising phase.

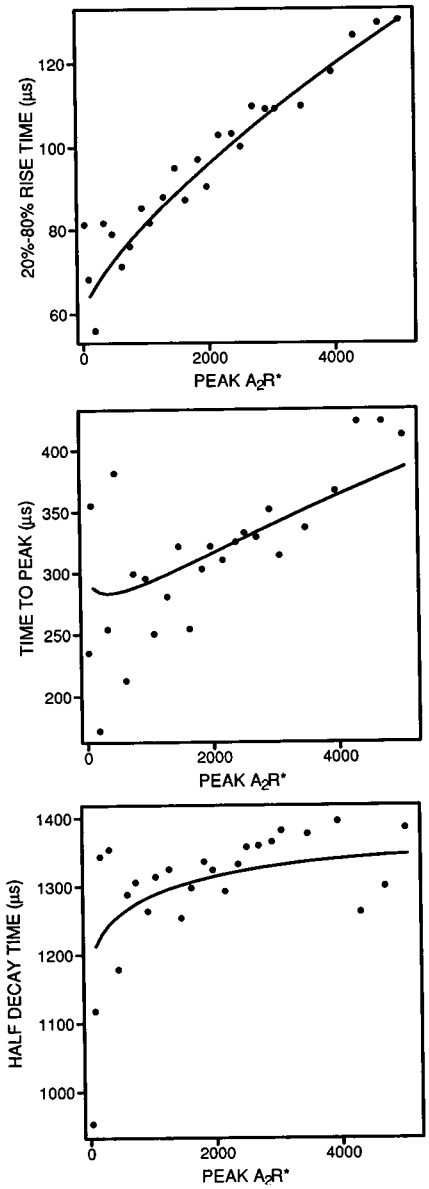

FIGURE 4 Temporal characteristics of simulated MEPCs at an active zone without a secondary cleft. In each graph, the filled circles are the results of the Monte Carlo simulations and the line is the results from the deterministic model. (*A*) The rise time (time between 20% and 80% of the peak value) for different size MEPCs (peak A_2R^*) due to the secretion of 1,000 to 30,000 ACh molecules in a quantum; the slope of the linear regression on the Monte Carlo data is about 1 μs/80 A_2R^*. (*B*) Time to peak (interval between the foot of the MEPC and its peak) for different size MEPCs; the slope of the linear portion of the line is about 1 μs/45 A_2R^*. (*C*) Time to half-decay of MEPCs of different amplitude.

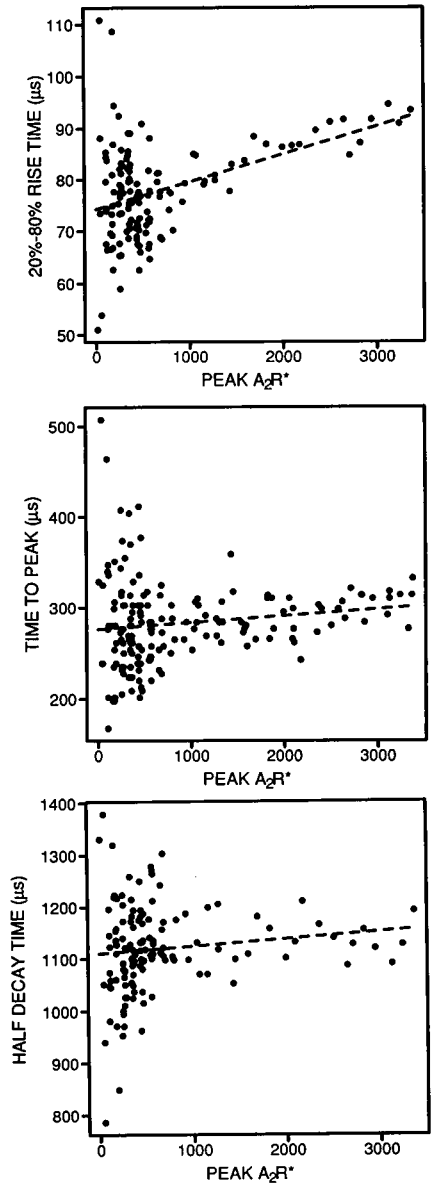

FIGURE 5 Temporal characteristics of simulated MEPCs at an active zone with secondary clefts. In each graph, the filled circles are from the Monte Carlo simulations and the broken line is the linear regression on these data. (*A*) Rise time for different size MEPCs due to the secretion of 1,000 to 30,000 ACh molecules in a quantum; the regression line has a gradient of 1 μs/185 A_2R^*. (*B*) Time to peak for different sized MEPCs; the regression line has a gradient of 1 μs/135 A_2R^*. (*C*) Time to half-decay for MEPCs of different amplitude; the regression line has a gradient of 1 μs/73 A_2R^*.

their absence makes a significant difference in the relationship between the temporal characteristics of the junctional currents and the amount of ACh in a quantum.

Relation between the amplitude of quantal currents and the amount of ACh in a quantum

The question next arises as to the quantitative relationship between the peak size of the MEPCs (that is, the peak A_2R^*) and the amount of ACh in a quantum. It might be expected that this would be highly nonlinear, as it is well established that potentiation of MEPCs occurs when there is overlap in the effects of quanta released simultaneously from adjacent release sites (see Introduction). The surprising result obtained was that there is an approximately linear relationship between the peak size of the MEPCs and the amount of ACh in a quantum in the range from about 4000 to 30,000 molecules for both end plates without secondary clefts (Fig. 6 *A*) and those with secondary clefts (Fig. 6 *B*).

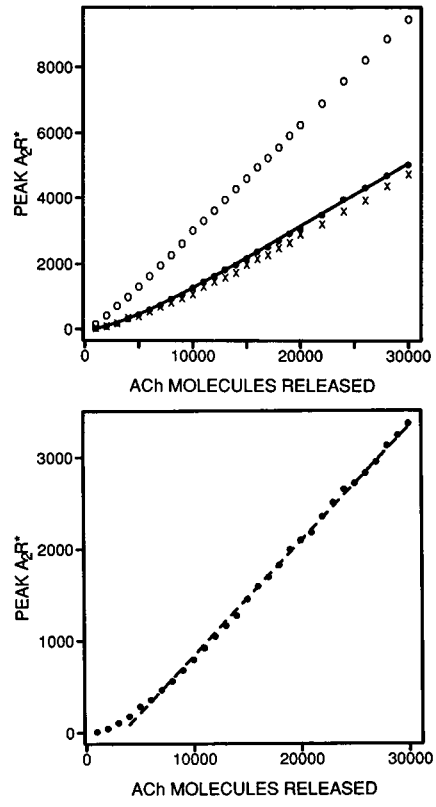

FIGURE 6 Amplitude of the peak MEPC (peak A_2R^*) for different amounts of ACh in a quantum. (*A*) Active zones without secondary clefts. Filled circles give the results for a given number of ACh molecules according to the stochastic model, and the line is the result for the deterministic model. The gradient of the line above about 4000 ACh is 1 A_2R^*/5.5 ACh molecules. The crosses are according to the full three-stage model of Eq. 1. The open circles are according to the full three-stage model of Eq. 1 using the parameter values given in Auerbach (1993). (*B*) Active zones with secondary clefts. Filled circles are the results for a given number of ACh molecules according to the stochastic model; the broken line is the regression line to these for 4000 ACh and above, and has a gradient of about 1 A_2R^*/8 ACh molecules.

Significant nonlinear effects were evident, however, at MEPC sizes less than 4000 to 5000 ACh molecules in both cases (Fig. 6). The stochastic variation in the peak A_2R^* responses in this range of ACh for the case without secondary clefts is given in Table 2.

To check that these result were not dependent on using the simplified two-step model of Eq. 2, solutions were obtained for the full three-step model given by Eq. 1. There was no significant difference between the results for the two solutions (Fig. 6 *A*). An additional possibility that the linearity of the relation between peak A_2R^* and the amount of ACh in a quantum above about 4000 molecules arises from the kinetic parameters chosen was checked. The kinetic parameters of Auerbach (1993), rather than those of Bartol et al. (1991), were used in Eq. 1 (see Table 1). Fig 6 *A* shows that the Auerbach (1993) parameters gave an even more linear relation for peak A_2R^* versus the amount of ACh in a quantum.

TABLE 2 Mean and standard deviation in the peak number of A_2R^* for a range of ACh

Molecules of ACh	Mean peak (A_2R^*)	SD peak (A_2R^*)
250	1.65	1.35
500	7.80	2.46
1000	25.85	3.95
2500	125.35	9.61
5000	396.85	16.40

Monte Carlo calculations for an end plate without secondary clefts, 20 runs for each case.

To investigate the origins of this linear relationship further, the kinetic equations Eqs. 4 to 10 were solved for the interaction between ACh (A), acetylcholine receptors (R), and cholinesterase (E) when these are allowed to freely mix in a homogeneous chemical reaction not bound to membranes or constrained by any particular geometry. The peak A_2R concentration reached in the reaction for a particular initial ACh concentration $[A]_0$ was calculated. The results show that if the initial amounts of R and E are increased in proportion to the increase in initial A, there is a linear relationship between the peak A_2R and the initial ACh concentration (Fig. 7 *B*); this is in contrast with the case in which there is a constant amount of R and E at the beginning of the reaction, so that the amount of A_2R formed reaches saturation as initial A is increased (Fig. 7 *A*). From these results, a likely explanation for the linear relationship between the peak amplitude of the MEPCs and the ACh in a quantum is that as the amount of ACh in the quantum increases there is an increase in the access of the ACh to the substrates with which it reacts, and to a first approximation this can be modeled as a homogeneous chemical reaction.

Conditions under which amplitude histograms of quantal currents might reveal subunits in the quantum of ACh release

As mentioned in the Introduction, it is possible that ACh release occurs in subunits that are only a fraction of the amount of ACh in a quantum. If this is the case, then the conditions under which it might be detected need to be established. Amplitude-frequency histograms of MEPCs are one way that has been used to try to detect whether transmitter is released in subunits. It has been claimed that this is not likely to be a very effective way of determining that the quantum has a subunit structure as one subunit released soon after another will be potentiated in its response and so lead to a loss in detectable subunit structure in the amplitude-frequency histogram of MEPCs. However, the previous section shows that such potentiation is slight for multiples of subunits involving a total of more than about 4000 ACh molecules, so that it is worthwhile to examine the possibility further. To do this, the stochastic equations have been solved for 500 MEPCs generated at end plates with secondary clefts; the subunit size has been taken as 1000 ACh molecules and the number of subunits in a quantum

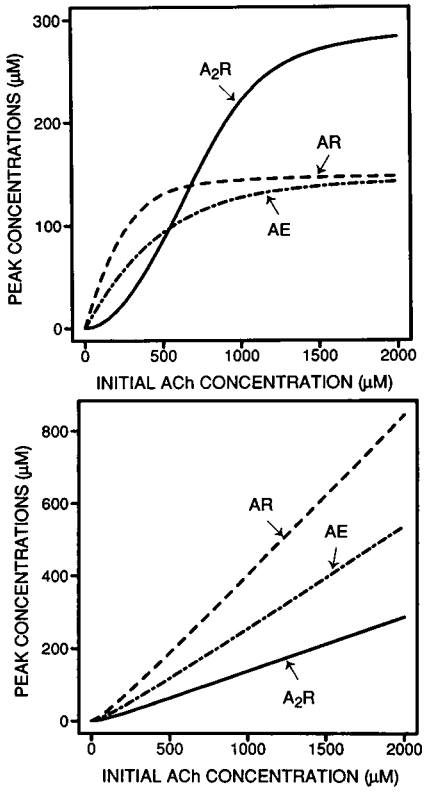

FIGURE 7 The peak amount of products formed in a homogeneous solution consisting of ACh (A), ACh receptors (R), and cholinesterase molecules (E), as a function of the initial ACh concentration. (*A*) Case in which the initial concentration of ACh receptors as well as initial cholinesterase are constant (at 300 μM and 150 μM, respectively). The kinetic equations 4 to 10 were used to calculate the peak concentrations of A_2R (*continuous line*), AR (*dashed line*), and AE (*dot-dashed line*) reached for a particular initial ACh concentration. (*B*) Case in which the initial concentrations of ACh receptors and cholinesterase are increased in proportion to the increase in initial ACh (proportionality constants 1 and 0.5, respectively). In this case, solution of the kinetic equations 4 to 10 gives a linear relationship between the peak A_2R (*continuous line*), peak AR (*dashed line*), and peak AE (*dot-dashed line*) and the initial ACh.

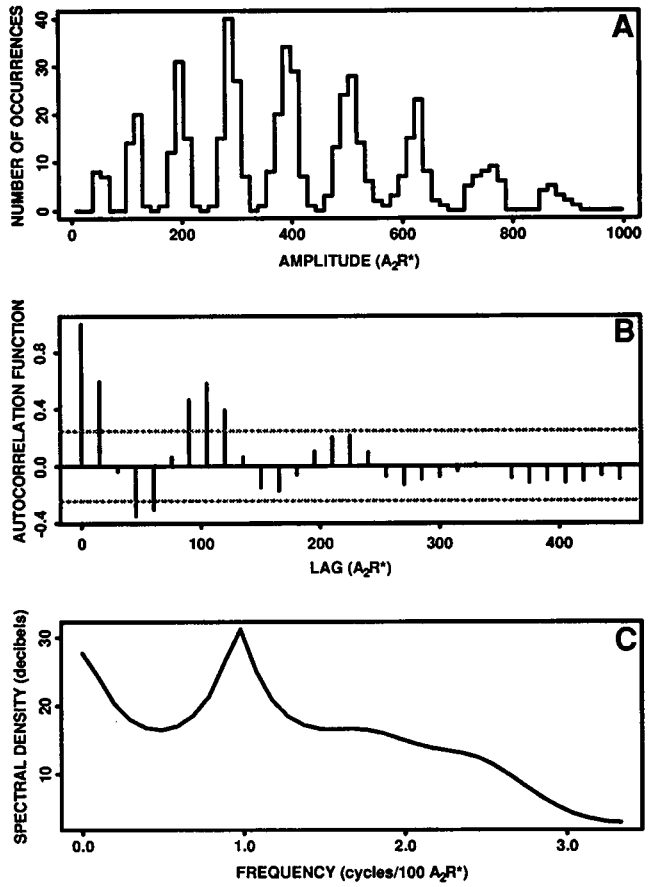

FIGURE 8 Analysis of the results of 500 Monte Carlo simulations of the MEPC at an end plate with secondary clefts in which the subunit size was fixed at 1000 ACh molecules. Groups of between 2 and 10 subunits were simultaneously released, the actual number being found from a binomial distribution with $n = 18$ and $p = 0.33$. (*A*) Amplitude-frequency histogram for the peak number of open channels (A_2R^*), using a bin size of 15. (*B*) Autocorrelation function for the histogram in *A* (the broken line indicates the 95% confidence limit); this indicates a periodicity in the histogram of about 100 open channels. (*C*) Spectral density for the histogram in *A*; this shows a clear peak indicating a periodic component corresponding to about 100 open channels. Thus both analyses confirm that the subunits can be detected in the histogram. The graphs in *B* and *C* were produced using the statistical package Splus.

drawn from a binomial distribution with an n of 18 and a p of 0.33. The amplitude-frequency histogram of these 500 MEPCs shows quite discrete bumps, indicating the existence of subunits (Fig. 8 *A*). Objective evaluation of this fact is provided by the use of both an autocorrelation analysis of the histogram (Fig. 8 *B*) and a spectral density analysis of the histogram (Fig. 8 *C*). In both of these, clear peaks occur, indicating the existence of a subunit structure in the histogram.

The question arises as to whether a smaller subunit size, such as 300 ACh molecules, which would only involve the summation of subunits in the nonlinear range (that is, less than 4000 molecules; see Fig. 6 *A*), could be detected in amplitude-frequency histograms of MEPCs. The simulation of Fig. 9 shows that a subunit structure to the histogram can still be detected in the spectrum. The existence of such a small subunit (300 ACh molecules) can be much more easily ascertained if the kinetic parameters of Auerbach (1993; see Table 1) are used in preference to those of Bartol et al. (1991). In this case, both the autocorrelation and spectral density show very distinctively a subunit structure, which can also be easily detected by eye (Fig. 10).

Any subunit is likely to have variance associated with it. This will have the effect of smearing out the bumps in the amplitude-frequency histograms for the MEPCs consisting of a relatively large number of subunits. Such effects arise if the subunits are independent, so that if there are n subunits in a quantum then the variance for that quantum is n times the variance of a single subunit. The amplitude-frequency histogram in Fig. 11 *A* was obtained for the case in which the subunit size was drawn from a normal distribution of mean of 1000 ACh molecules and this had a standard deviation of 50 ACh molecules; again, 500 quanta were released and each of these

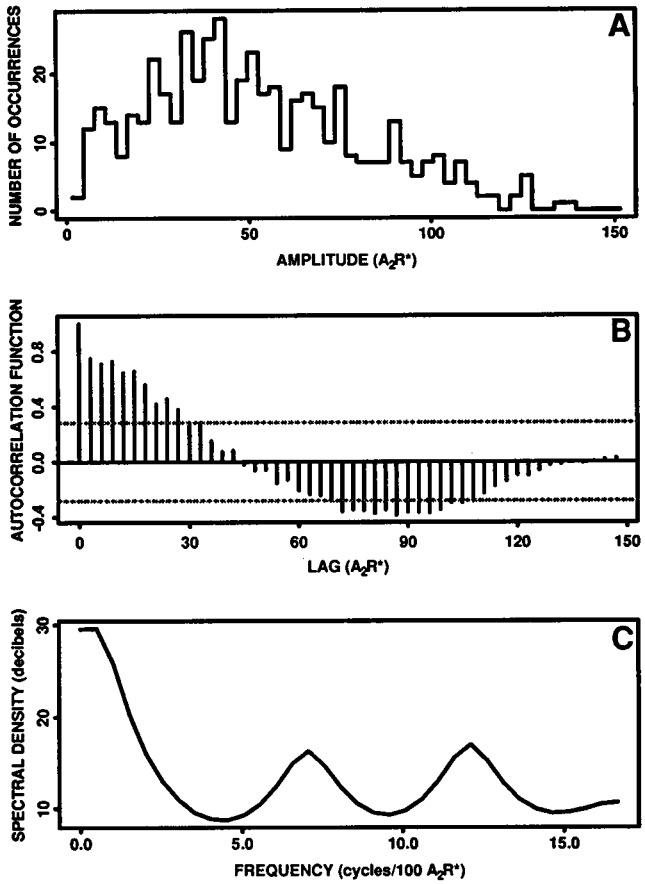

FIGURE 9 Analysis of the results of 500 Monte Carlo simulations of the MEPC at an end plate with secondary clefts in which the subunit size was fixed at 300 ACh molecules. Groups of between 2 and 10 subunits were simultaneously released, the actual number being found from a binomial distribution with $n = 18$ and $p = 0.33$. (*A*) Amplitude-frequency histogram for the peak number of open channels (A_2R^*), using a bin size of 3. (*B*) Autocorrelation function for the histogram in *A* (the broken line indicates the 95% confidence limit); this does not detect any subunit structure in the histogram. (*C*) Spectral density for the histogram in *A*; this shows two clear peaks, the first of which indicates a periodic component corresponding to about 14 open channels. (The second peak arises from the overlap of responses to the integer multiples of subunits.) The graphs in *B* and *C* were produced using the statistical package Splus.

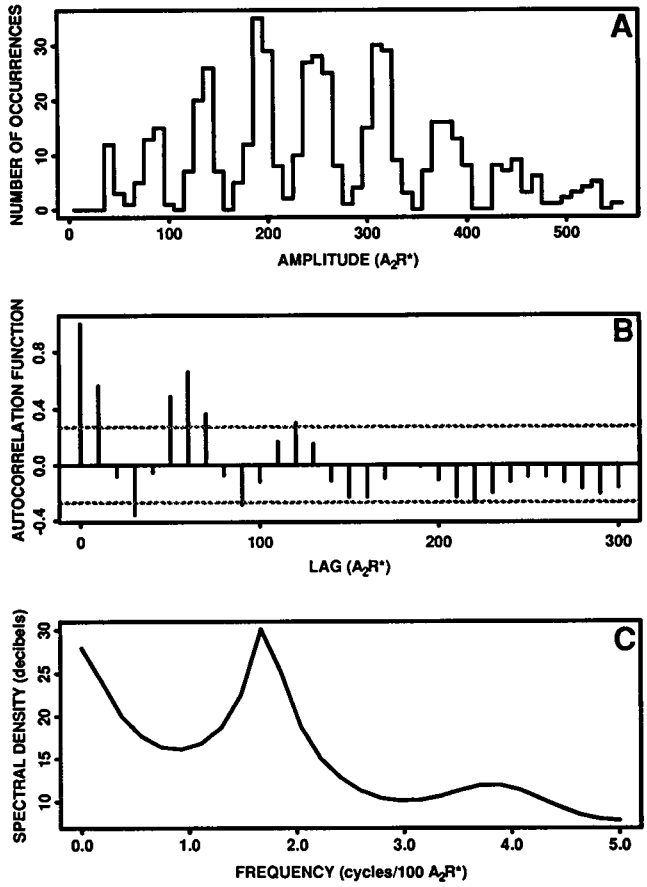

FIGURE 10 Analysis of the results of 500 Monte Carlo simulations of the MEPC at an end plate with secondary clefts in which the subunit size was fixed at 300 ACh molecules and the kinetic parameters in the simulations were from Auerbach (1993). Groups of between 2 and 10 subunits were simultaneously released, the actual number being found from a binomial distribution with $n = 18$ and $p = 0.33$. (*A*) Amplitude-frequency histogram for the peak number of open channels (A_2R^*), using a bin size of 10. (*B*) Autocorrelation function for the histogram in *A* (the broken line indicates the 95% confidence limit); this indicates a periodicity in the histogram of about 60 open channels. (*C*) Spectral density for the histogram in *A*; this shows a clear peak indicating a periodic component corresponding to about 60 open channels. Thus both analyses confirm that the subunits can be detected in the histogram. The graphs in *B* and *C* were produced using the statistical package Splus.

had a number of subunits drawn from a binomial distribution with an n of 18 and a p of 0.33. Bumps are still discernible in the histogram of MEPC amplitudes (Fig. 11 *A*), and this is supported by both the autocorrelation graph (Fig. 11 *B*) and the spectral density graph (Fig. 11 *C*) for the histogram, each of which shows peaks, indicating that the histogram has a still discernible subunit structure. In some experimental situations the amplitude-frequency histogram of MEPCs is not as wide as that in Fig. 11. To check that subunits could be detected in such histograms, these were drawn from a normal distribution as in Fig. 11, but the numbers of subunits released were obtained from a binomial distribution with an n of 9 and a p of 0.67, giving the narrower histogram of Fig. 12. It can be seen that both autocorrelation and spectral density detected a subunit response size of about 100 A_2R^*.

There is of course a limit to the amount of variance in the subunit size that will still allow the detection of subunits in the amplitude-frequency histograms. For instance, if the standard deviation of the subunit size is increased to 100 molecules with a mean size of 1000 molecules, then the amplitude-frequency histogram shows bumps (Fig. 13 *A*) that are just detectable as subunits in the autocorrelation (Fig. 13 *B*) and the spectral density (Fig. 13 *C*). Some insight into the way increasing the variance of the subunits effects the evidence for them in the amplitude-frequency histogram of MEPCs can be found by simple addition of random variables as given in Eqs. 10 and 11. For the choice $n = 18$, $p = 0.33$, $\mu = 1$ the density function $f_W(w)$ was calculated for a number of values of σ and the height of the

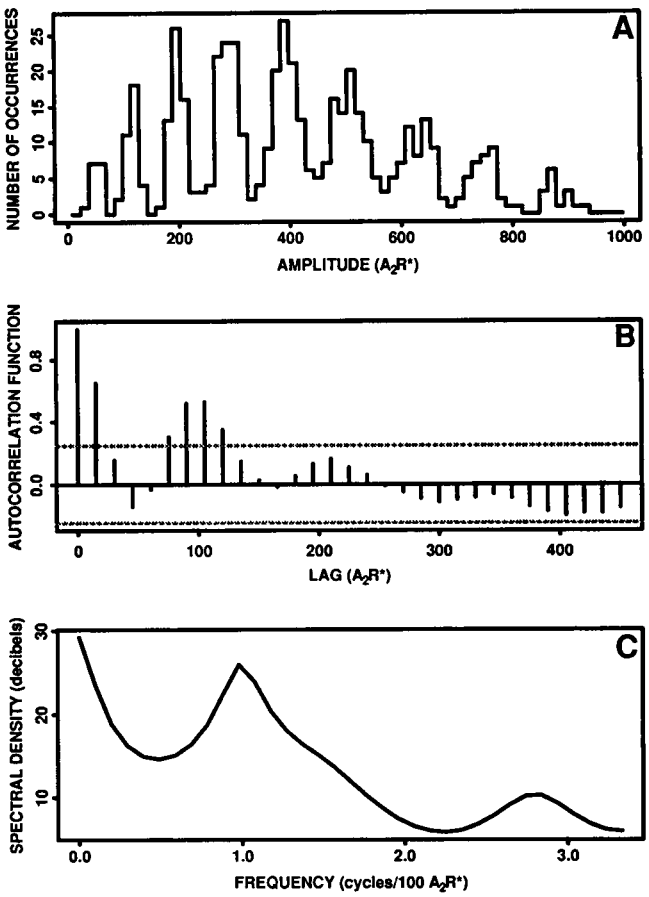

FIGURE 11 As for Fig. 8, except that the subunit size is now drawn from a Gaussian distribution of mean 1000 and standard deviation 50. The autocorrelation and spectral density still clearly indicate that the subunit is detectable in the histogram.

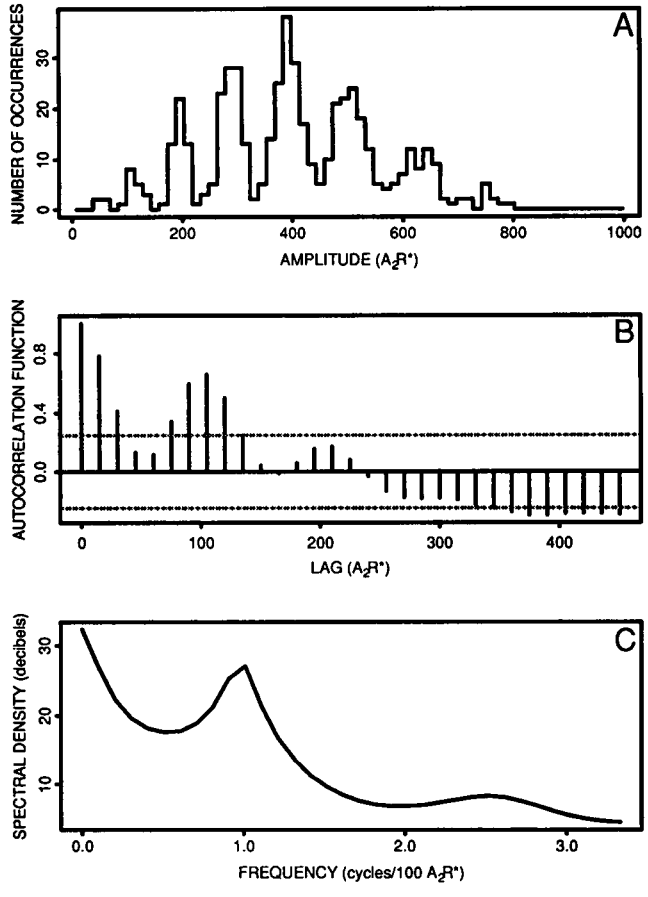

FIGURE 12 As for Fig. 8, except that the subunit size is now drawn from a Gaussian distribution of mean 1000 and standard deviation 50, and groups of between 2 and 10 subunits were simultaneously released, the actual number being found from a binomial distribution with $n = 9$ and $p = 0.67$. The autocorrelation and spectral density still clearly indicate that a subunit response of about 100 open channels is detectable in the histogram.

first peak in the spectrum was measured. The results in Fig. 14 show that for $\sigma > \sim 0.16$ it is unlikely that the amplitude-frequency histogram will provide any evidence for a subunit structure in the quantum. Note that σ will contain variability due to both the subunit size and the diffusion and binding processes. Analysis of the Monte Carlo results for fixed subunit size (1000 molecules) indicates that the diffusion and binding contributes about 0.05 to σ, so the maximum contribution to σ from subunit size variation will be of the order of 0.1. Fig. 13 indicates that for a coefficient of variation of 0.1 the subunit structure is still just evident.

In addition, instrumental noise will add to the variance, as represented by the term Z in Eq. 15. The choice $\tilde{\sigma} = 0.2$ gives the additional reduction shown by the second curve in Fig. 14. The overall conclusion is that subunits will probably become experimentally undetectable about the time the coefficient of variation for their size reaches 0.1. It is interesting to note that a similar conclusion was reached in discussions on this detection problem by Magleby and Miller (1981), Matteson et al. (1981), as well as by Edwards et al. (1990).

The effect of sequential release of subunits in a quantum of ACh on the time course and amplitude histograms of the quantal currents

If the quantum does consist of subunits then they might not be released simultaneously, as assumed above, but sequentially at some regular interval. This interval cannot be too large; otherwise the rise time of the MEPC will increase with an increase in their size at a rate greater than the small amount that is observed experimentally, and this is already mostly accounted for by the diffusion of ACh and its reactions with AChR and cholinesterase (Fig. 5 *A*). The effects of releasing subunits in a quantum at intervals of 5 μs on the temporal characteristics of the MEPC with an increase in the number of subunits in the quantum is shown in Fig. 15: as expected, there is a relatively small change in the time for half-decay of the MEPC with an increase in its amplitude over that seen during synchronous release (1 μs/104 A_2R^* in Fig. 15 *C* compared with 1 μs/73 A_2R^* in Fig. 5 *C*), whereas the rise time increases at a greater rate with an increase in the number of subunits in the MEPC (1 μs/88

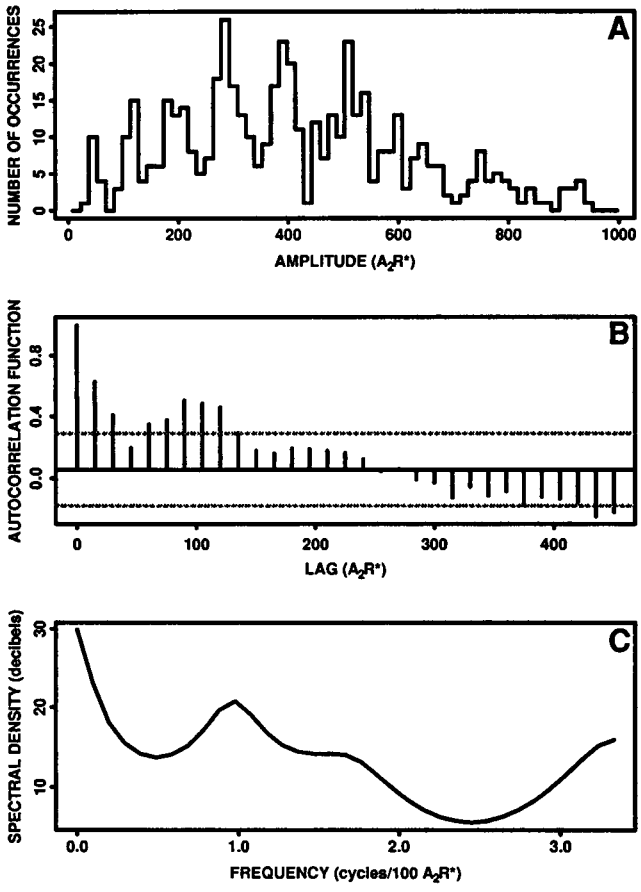

FIGURE 13 As for Fig. 8, except that the subunit size is now drawn from a Gaussian distribution of mean 1000 and standard deviation 100. The autocorrelation and spectral density still indicate that the subunit is just detectable in the histogram, although it should be noted that there is a considerable reduction in the peak in the spectral density.

A_2R^* in Fig. 15 *A* compared with 1 μs/185 A_2R^* in Fig. 5 *A*), as does the time to peak (1 μs/35 A_2R^* (Fig. 15 *B*) compared with 1 μs/135 A_2R (Fig. 5 *C*).

If sequential release of subunits does occur it might still be possible to detect the subunits in the amplitude-frequency histogram of MEPCs. Fig. 16 shows a histogram of 500 MEPCs in which subunits are released at 5-μs intervals in each quantum; the subunit has a mean of 1000 ACh molecules with a standard deviation of 50 molecules, and the number of subunits in a quantum is drawn from a binomial distribution with an n of 80 and a p of 0.33. The subunit structure of the quantum still shows up clearly in the bumps of the histogram (Fig. 16 *A*), and this is reinforced by the clear indication of the subunits in both the autocorrelation and spectral density analysis (Fig. 16 *B* and 16 *C*). The release of subunits at intervals greater than 5 μs, although not realistic in terms of giving an experimentally verifiable rate of increase of MEPC rise time with amplitude, actually enhances detection of the subunit structure in the amplitude-frequency histograms of MEPCs, as shown in Fig. 17 for the case in which subunits are released at intervals of 20 μs (compare with Fig. 16).

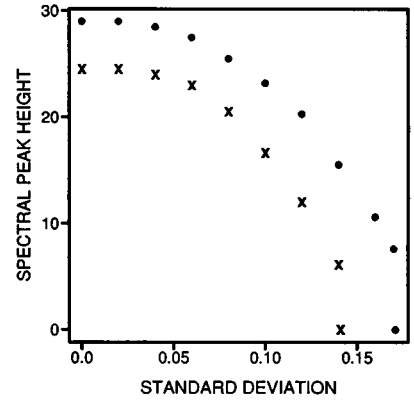

FIGURE 14 Relationship between the height of the major peak in the spectral density and the variance of the subunit size for amplitude-frequency histograms of the kind shown in Figs. 11 and 13. This graph, however, was not generated by simulation; rather, it was found by the summation of N random variables X_i according to Eqs. 16 and 17. N is binomially distributed with parameters $n = 18$, $p = 0.33$; X_i is normally distributed with mean $\mu = 1$ and standard deviation σ. The filled circles show the height of the principal spectral peak (relative to the minimum preceding it) as a function of the standard deviation σ of X_i. The crosses are for the same calculation with the addition of an experimental noise term Z, with mean 0 and standard deviation 0.2.

There is a subclass of MEPCs that have a much slower rate of rise and sometimes decay than the large majority of MEPCs (see Introduction). These could occur if the subunits that compose the quantum are occasionally released asynchronously at different intervals. It is a simple matter to generate such MEPCs by increasing the interval between the release of subunits in arbitrary ways that will simulate any required pattern of temporal characteristics of the MEPC. An example of such an unusual MEPC generated in this way is shown in Figs. 3 *C* and 3 *D* (compare with figure 9 in Girod et al., 1993). It is possible to simulate more extended sets of inflections on the rising or falling phases of the MEPC.

Analysis of an amplitude-frequency histogram of MEPCs recorded from a small group of active zones

Recordings were made of MEPCs with small-diameter extracellular electrodes (about 6 μm) placed in the loose-patch mode over selected regions of visualized amphibian motor-nerve terminal branches. Up to 1000 MEPCs were observed, and amplitude-frequency histograms of these were constructed as in Fig. 18 *A*. This shows a histogram that was particularly broad and showed marked fluctuations. However, both autocorrelation (Fig. 18 *B*) and spectral density analysis (Fig. 18 *C*) failed to provide evidence for a subunit component in the histogram.

DISCUSSION

The time course of quantal currents

As the mean size of MEPCs is about 5 nA at end plates with secondary clefts (Hartzell et al., 1975; Land et al., 1981;

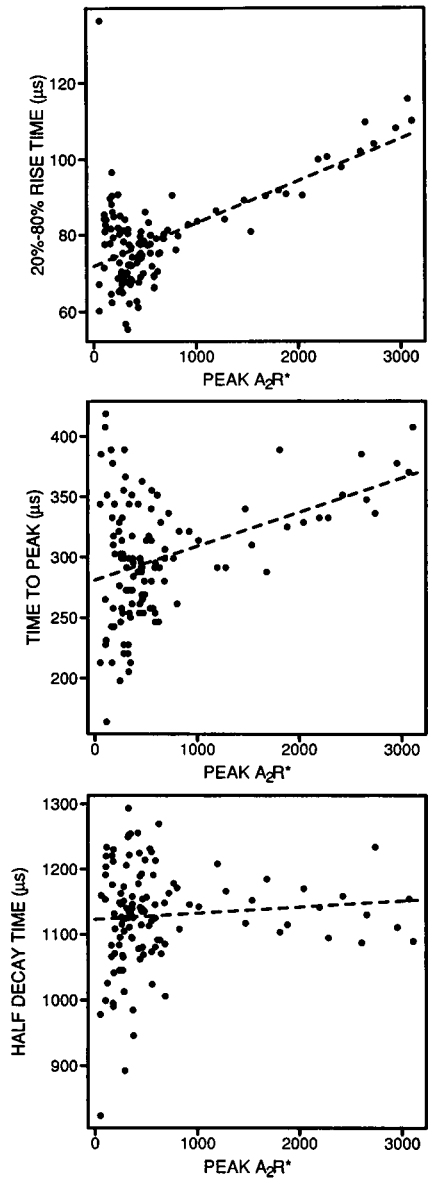

FIGURE 15 Temporal characteristics of simulated MEPCs at an active zone with secondary clefts when the subunits in a quantum are released at intervals of 5 μs. In each graph, the filled circles are from the Monte Carlo simulations and the broken line is the linear regression on these data. (*A*) Rise time for different-sized MEPCs due to the secretion of 1,000 to 30,000 ACh molecules in a quantum; the regression line has a gradient of 1 μs/88 A_2R^*. (*B*) Time to peak for different-sized MEPCs; the regression line has a gradient of 1 μs/35 A_2R^*. (*C*) Time to half-decay for MEPCs of different amplitude; the regression line has a gradient of 1 μs/105 A_2R^*.

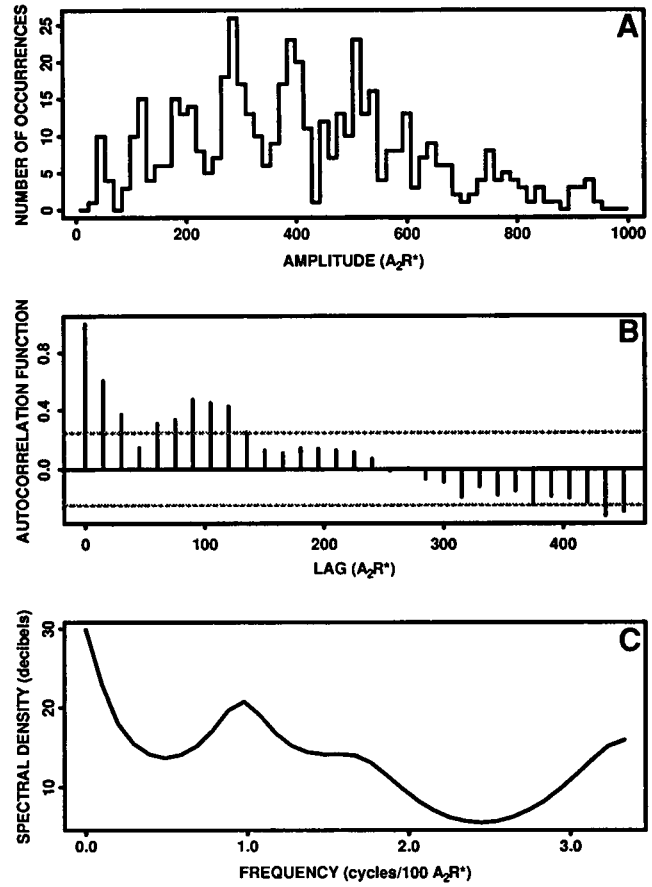

FIGURE 16 As for Fig. 8, except that the subunit size is now drawn from a Gaussian distribution of mean 1000 and standard deviation 50, and the individual subunits in each group were released sequentially with an interval of 5 μs between releases. The autocorrelation and spectral density still clearly indicate that the subunit is detectable in the histogram.

Erxleben and Kriebel, 1988) and each open channel passes a current of about 3 pA (Hamill and Sakmann, 1981), then there must be about 1700 open channels, A_2R^*. Fig. 5 indicates that this number of A_2R^* gives a MEPC with a rise time of about 85 μs, a time to peak of about 300 μs, and a half-decay time of about 1110 μs. Land et al. (1981) obtained a rise time of 90 μs for the MEPC at the lizard end plate. The forward binding rate constant for acetylcholine at the end plate used in the stochastic model has been determined by Land et al. (1981) on the basis of a rise time of 100 μs, so that it is a tautology to say that the stochastic model predicts the rise time. These rise times are substantially smaller than those of about 260 μs given for the mouse neuromuscular junction (Erxleben and Kriebel, 1988), and the time to peak of 300 μs is substantially smaller than the 500 to 1000 μs measured by Vautrin and Kriebel (1991) for this end plate, but about the same as that recently obtained for the frog end plate (about 300 μs; Cherki-Vakil et al., 1995). The theoretical half-decay time of 1110 μs is similar to the 1200 μs measured for the MEPC at the lizard end plate (Land et al., 1984), 1400 μs at the amphibian end plate (Katz and Miledi, 1973), 1200 μs at the snake end plate (Hartzell et al., 1975), and 900 μs (Linder et al., 1984) or 1100 μs (Erxleben and Kriebel, 1988) at the mouse end plate. In the case of end plates without secondary clefts, such as those of the electroplaque, the theoretical value for the time to peak was 360 μs for a mean-size MEPC of 12 nA (from Fig. 4 *B*) compared with the measured value of 430 μs (Girod et al., 1993), and the theoretical value for the half-decay time was 1350 μs (from Fig.

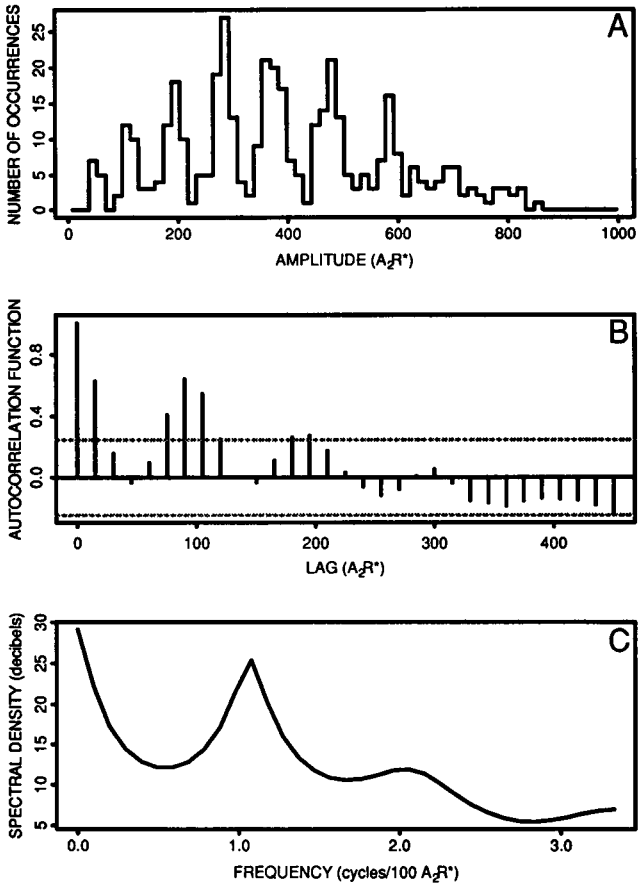

FIGURE 17 As for Fig. 8, except that the subunit size is now drawn from a Gaussian distribution of mean 1000 and standard deviation 50, and the individual subunits in each group were released sequentially with an interval of 20 μs between releases. The autocorrelation and spectral density still clearly indicate that the subunit is detectable in the histogram.

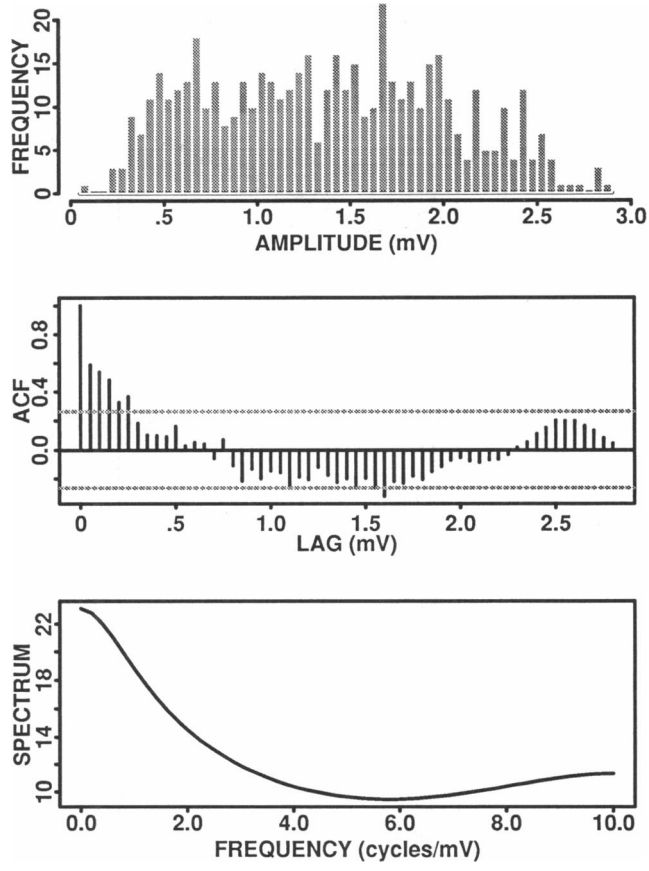

FIGURE 18 Analysis of 517 MEPCs recorded with a 6-μm external electrode placed in the loose-patch mode over a section of visualized motor-terminal branch of the iliofibularis muscle of a toad (*Bufo marinus*). (*A*) Amplitude-frequency histogram of the MEPCs using a bin size of 0.05 mV. (*B*) Autocorrelation function for the histogram in *A* (the broken line indicates the 95% confidence limit); there is no evidence for periodicity in the histogram according to this criterion. (*C*) Spectral density for the histogram in *A*; there are no peaks present that could indicate a periodic component. Thus both analyses fail to suggest the existence of subunits in this histogram.

4 *C*) compared with the surprisingly small experimental value of 450 μs.

A very small positive increase in the rise time of the MEPC with an increase in the amplitude of the MEPC, due to an increase in the amount of ACh released in the quantum, has been reported for the mouse by Erxleben and Kriebel (1988; about 1 μs/330 A2R*) as well as for the lizard by Land et al. (1984; 1 μs/330 A2R*), but was not detected in the frog by Vautrin and Kriebel (1991). Such a positive correlation is clearly evident at junctions of electroplaques (Figs. 3 *B* and 4 *C* in Girod et al., 1993) for which a theoretical gradient of 1 μs/40 A2R* was obtained by Girod et al. (1993: their figure 8 *F*) using the deterministic equations of Wathey et al. (1979); this may be compared to the gradient obtained in the present work using either stochastic or deterministic equations (Fig. 4 *A*) of 1 μs/80 A_2R^* for MEPCs in the range of 1000 to 3000 A_2R^*. Both the deterministic and stochastic models of transmitter action predict a steeper gradient for the relationship between time to peak of the MEPC and their amplitude in the case of electroplaques than that for other end plates, and this seems to be borne out experimentally by the steep gradients observed in the electroplaque compared with that at the mouse and reptilian end plates. These gradients are greatly enhanced by inhibiting cholinesterase, presumably because of the increase in the number of occasions for which individual diffusing ACh molecules make repeated contact with the receptors (Katz and Miledi, 1973). A small positive increase in the time constant of decay with an increase in the MEPC was obtained with the stochastic model (Fig. 5 *C*), as has been observed at the mouse end plate (Erxleben and Kriebel, 1988; Linder et al., 1984) but not at the lizard end plate (Land et al., 1984).

The question arises as to what extent asynchronous release of transmitter in a quantum is consistent with the above characteristics of the MEPC. The discharge of transmitter that constitutes a quantum must occur in less than 50 to 75 μs if the concentration of ACh is to be raised to a level over the postsynaptic receptors sufficient to give the characteristics of the MEPC (Khanin et al., 1994). If 10 subunits

of ACh make up a quantum, then each of these must then be released in less than 10 μs. The present work shows that increasing the interval between subunits between 5 μs and 20 μs increases the detection of subunits in the amplitude-frequency histograms of MEPCs. The addition of 100 μs to the rise time of the MEPC, taken to be 100 μs in the model calculations of Land et al. (1981), would change the estimations for the forward binding constant. However, the wide range of estimates for the rise time of the MEPC mentioned above (over 200 μs) indicates that this might not be a firmly established value.

There is a nearly linear relationship between the peak current generated during the MEPC and the number of subunits released in the range from about 4 to 30 (each composed of 1000 ACh molecules). If transmitter release does occur in subunits, there will not be a substantial contribution of potentiation to the relationship between the rise time of the MEPC and its amplitude or between the half-decay time of the MEPC and its amplitude. The existence of only a slight increase or the lack of increase in either the rise time or the time to decline with an increase in amplitude measured experimentally is not inconsistent with the quantum being composed of subunits. This conclusion seems to be at variance with that arrived at on theoretical grounds for the nerve electroplaque (Girod et al., 1993): there, synchronous release of subunits was calculated to give rise to an increase in the gradients relating the time to peak and the half-decay time, with an increase in the number of subunits released, of about 1 μs for each extra 20 channels opened by the addition of subunits to the quantum (their figure 8 *F*). These calculations are much the same as those in the present work for the end plate (Fig. 4 *A*). The present work shows that the existence of these gradients relating the rise time and decay time of the MEPC to its amplitude is not conditional on potentiating effects, as these are slight over a considerable range of A_2R^* for which there are significant changes in the rise time and decay time of the MEPC.

At the nerve-electroplaque junction there is a gradient between the time to peak and the amplitude of the MEPC that is clearly much greater than that observed at the end plate (compare figure 4 *C* in Girod et al., 1993 with figure 2 in Land et al., 1981 and figure 5 *B* in Erxleben and Kriebel, 1988). The same is the case for the half-decay time (compare figure 4 *A* in Girod et al., 1993 with figures 3 *B* and 10 *C* in Linder et al., 1984 and with figure 5 *C* in Erxleben and Kriebel, 1988). This has been used by Girod et al. (1993) to argue for a subunit structure to the quantum; they suggest that the difference in the gradients between the neuromuscular junction and the electroplaque junction arises because ACh subunits do not interact at the neuromuscular junction in the presence of cholinesterase as they do at the electroplaque. Girod et al. (1993) arrived at the conclusion that the positive gradients between time to peak and amplitude of the MEPC arise because of the potentiating effects of one subunit of ACh acting on the same receptors as an immediately preceding subunit. This idea was arrived at by comparing the A_2R generated by a subunit of 1000 ACh molecules in a quantum with that generated by five subunits in a quantum (that is, 5000 ACh molecules; their figure 8) and then extrapolating this effect to greater numbers of subunits in a quantum. As the present work shows (Figs. 4 *B* and 6 *A*), this range of 1000 to 5000 ACh molecules in a quantum is in the potentiating region of the curve relating A_2R to the number of ACh molecules, so that the results for the five-subunit release is much greater than five times the result for one-subunit release. However, these potentiating effects are slight beyond about 5000 ACh molecules, so that variation in the number of subunits from five to larger numbers of subunits in a quantum, each subunit consisting of 1000 ACh molecules, does not give rise to nonlinear changes in the number of A_2R generated. Positive gradients relating time to peak and amplitude of MEPCs do not arise from the potentiating effects of a subunit of ACh acting on the same receptors as a previous subunit. The experimental discovery of such gradients cannot then be used as evidence in favor of the subunit hypothesis, as the gradients exist independently of any subunit structure in the quantum.

The different shapes of MEPCs can easily be accommodated within the subunit hypothesis as being due to different patterns of asynchronous release, as has been argued quantitatively for the MEPCs at the electroplaque (Girod et al., 1993), for synaptic currents at hippocampal synapses (Vautrin et al., 1993), and in the present work for the end plate. The factors that might give rise to such large intervals between subunits released during the secretion of a quantum can only be identified when more knowledge is forthcoming concerning the mechanism of exocytosis (Monk and Fernandez, 1994).

The amplitude of quantal currents

The present work shows that the problem of one subunit potentiating the effect of a subsequent subunit and thereby removing a subunit structure from the amplitude-frequency histograms need not arise, as there is only slight potentiation in the range of subunit releases from about 4 to 20 (for a subunit size of 1000 molecules). As a result, if the subunit of the quantum is of constant size (say 1000 ACh molecules), then the stochastic model shows that peaks do occur in the amplitude-frequency histogram of MEPCs that coincide with the number of subunits released, as supported by both the autocorrelation and spectral analysis of the histograms. Furthermore, these peaks are still present if the subunits are released sequentially at intervals of about 5 to 20 μs.

Returning to the problem first raised by Katz (1977) concerning the variance of the hypothetical subunits, it is variance in the number of molecules in the subunits (as well as the fluctuations due to diffusion and binding of the transmitter and instrumental noise) that can remove the subunit peaks in the histograms. If the coefficient of variation of the subunit increases above about 0.1, then the

present work shows that neither autocorrelation nor spectral analysis can detect peaks in the histograms that might indicate a subunit structure in the quantum. This is a small variance and raises the question as to what near-deterministic release process could maintain such an exact subunit size.

Support under Australian Research Council grant AC9330365 is acknowledged.

REFERENCES

Auerbach, A. 1993. A statistical analysis of acetylcholine receptor activation in Xenopus myocytes: stepwise versus concerted models of gating. *J. Physiol.* 461:330–378.

Bartol, T. M., Jr., B. R. Land, E. E. Salpeter, and M. M. Salpeter. 1991. Monte Carlo simulation of miniature endplate current generation in the vertebrate neuromuscular junction. *Biophys. J.* 59:1290–1307.

Bennett, M. R. 1972. Autonomic Neuromuscular Transmission. Monographs of the Physiological Society. Cambridge University Press, Cambridge, England.

Bennett, M. R., P. Jones, and N. A. Lavidis. 1986. The probability of quantal secretion along visualized terminal branches at amphibian (*Bufo marinus*) neuromuscular synapses. *J. Physiol.* 379:257–274.

Bennett, M. R., and A. G. Pettigrew. 1975. The formation of synapses in amphibian striated muscle during development. *J. Physiol.* 252: 203–239.

Bevan, S. 1976. Sub-miniature end-plate potentials at untreated frog neuromuscular junctions. *J. Physiol.* 64:85–103.

Carlson, C. G., and M. E. Kriebel. 1985. Neostigmine increases the size of subunits composing the quantum of transmitter release at mouse neuromuscular junctions. *J. Physiol.* 367:489–502.

Cherki-Vakil, R., S. Ginsburg, and H. Meiri. 1995. The difference in shape of spontaneous and uniquantal evoked synaptic potentials in frog muscle. *J. Physiol.* 482:641–650.

Edwards, F. A., A. Konnerith, and B. Sakmann. 1990. Quantal analysis of inhibitory synaptic transmission in the dentate gyrus of rat hippocampal slices: a patch clamp study. *J. Physiol.* 430:213–249.

Erxleben, C., and M. E. Kriebel. 1988. Characteristics of spontaneous miniature and subminiature endplate currents at the mouse neuromuscular junction. *J. Physiol.* 400:645–658.

Garcia-Segura, L. M., D. Muller, and Y. Dunant. 1986. Increase in the number of presynaptic large intermembrane particles during synaptic transmission at the Torpedo nerve-electroplaque junctions. *Neuroscience.* 19:63–79.

Girod, R., P. Corrèges, J. Jacquet, and Y. Dunant. 1993. Space and time characteristics of transmitter release at the nerve-electroplaque junction of Torpedo. *J. Physiol.* 471:129–157.

Hamill, O. P., and B. Sakmann. 1981. Multiple conductance states of single acetylcholine receptor channels in embryonic muscle cells. *Nature.* 294:462–464.

Hartzell, H. C., S. W. Kuffler, and D. Yoshikami. 1975. Post-synaptic potentiation: interaction between quanta of acetylcholine at the skeletal neuromuscular junction. *J. Physiol.* 251:427–463.

Heuser, J. E., and T. S. Reese. 1977. Structure of the synapse. *In* Handbook of Physiology, Sec. 1. The Nervous System. Vol. 1. E. R. Kandel, editor. American Physiological Society, Bethesda, MD. 261–294.

Katz, B. 1977. Prologue. *In* Synapses. G. A. Cottrell and D. N. R. Usherwood, editors. London, Academic Press. 1–5.

Katz, B., and R. J. Miledi. 1973. The binding of acetylcholine to receptors and its removal from the synaptic cleft. *J. Physiol.* 231:549–574.

Khanin, R., H. Parnas, and L. Segel. 1994. Diffusion cannot govern the discharge of neurotransmitter in fast synapses. *Biophys. J.* 67:966–972.

Kriebel, M. E., and C. E. Gross. 1974. Multimodal distribution of frog miniature endplate potentials in adult, denervated and tadpole leg muscle. *J. Gen. Physiol.* 64:85–103.

Kriebel, M. E., F. Llados, and D. R. Matteson. 1982. Histograms of the unitary evoked potential of the mouse diaphragm show multiple peaks. *J. Physiol.* 322:211–222.

Land, B. R., W. V. Harris, E. E. Salpeter, and M. M. Salpeter. 1984. Diffusion and binding constants for acetylcholine derived from the falling phase of miniature endplate currents. *Proc. Natl. Acad. Sci. USA.* 81:1594–1598.

Land, B. R., E. E. Salpeter, and M. M. Salpeter. 1980. Acetylcholine receptor density affects the rising phase of miniature endplate currents. *Proc. Natl. Acad. Sci. USA.* 77:3736–3740.

Land, B. R., E. E. Salpeter, and M. M. Salpeter. 1981. Kinetic parameters for acetylcholine interaction in intact neuromuscular junctions. *Proc. Natl. Acad. Sci. USA.* 78:7200–7204.

Linder, T. M., P. Pennefather, and D. M. J. Questel. 1984. The time course of miniature endplate currents and its modification by receptor blockade and ethanol. *J. Gen. Physiol.* 83:435–468.

Magleby, K. L., and D. C. Miller. 1981. Is the quantum of transmitter release composed of subunits? A critical analysis in the mouse and frog. *J. Physiol.* 311:267–287.

Matteson, D. R., M. E. Kriebel, and F. Llados. 1981. A statistical model indicates that miniature end-plate potentials and unitary evoked end-plate potentials are composed of subunits. *J. Physiol.* 90:337–363.

Monk, J. R., and J. M. Fernandez. 1994. The exocytotic fusion pore and neurotransmitter release. *Neuron.* 12:707–716.

Vautrin, J. 1986. Subunits in quantal transmission at the mouse neuromuscular junction: some tests of peak intervals in amplitude distributions. *J. Theor. Biol.* 120:363–370.

Vautrin, J., and M. E. Kriebel. 1991. Characteristics of slow-miniature end-plate currents show a subunit composition. *Neuroscience.* 41: 71–88.

Vautrin, J., A. E. Schaffner, B. Fantas, and J. L. Barker. 1993. Frequency modulation of transmitter release. *J. Physiol. (Paris).* 87:51–73.

Walrond, J. P., and T. S. Reese. 1985. Structure of axon terminals and active zones at synapses on lizard twitch and tonic muscle fibres. *J. Neurosci.* 5:1118–1131.

Wathey, J. C., M. M. Nass, and H. A. Lester. 1979. Numerical reconstruction of the quantal event of nicotinic synapses. *Biophys. J.* 27:145–164.